



**HAL**  
open science

# Quasi-geostrophic vortex vertical alignment in near collapse interactions

Jean N Reinaud, Xavier Carton

► **To cite this version:**

Jean N Reinaud, Xavier Carton. Quasi-geostrophic vortex vertical alignment in near collapse interactions. *Geophysical and Astrophysical Fluid Dynamics*, 2023, 117 (5), pp.292-314. 10.1080/03091929.2023.2242571 . hal-04837265

**HAL Id: hal-04837265**

**<https://univ-paris8.hal.science/hal-04837265v1>**

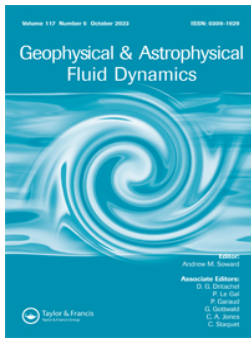
Submitted on 13 Dec 2024

**HAL** is a multi-disciplinary open access archive for the deposit and dissemination of scientific research documents, whether they are published or not. The documents may come from teaching and research institutions in France or abroad, or from public or private research centers.

L'archive ouverte pluridisciplinaire **HAL**, est destinée au dépôt et à la diffusion de documents scientifiques de niveau recherche, publiés ou non, émanant des établissements d'enseignement et de recherche français ou étrangers, des laboratoires publics ou privés.



Distributed under a Creative Commons Attribution 4.0 International License



## Quasi-geostrophic vortex vertical alignment in near collapse interactions

Jean N. Reinaud & Xavier Carton

**To cite this article:** Jean N. Reinaud & Xavier Carton (2023) Quasi-geostrophic vortex vertical alignment in near collapse interactions, *Geophysical & Astrophysical Fluid Dynamics*, 117:5, 292-314, DOI: [10.1080/03091929.2023.2242571](https://doi.org/10.1080/03091929.2023.2242571)

**To link to this article:** <https://doi.org/10.1080/03091929.2023.2242571>



© 2023 The Author(s). Published by Informa UK Limited, trading as Taylor & Francis Group.



Published online: 10 Aug 2023.



Submit your article to this journal [↗](#)



Article views: 427




View related articles [↗](#)



View Crossmark data [↗](#)

# Quasi-geostrophic vortex vertical alignment in near collapse interactions

Jean N. Reinaud <sup>a</sup> and Xavier Carton <sup>b</sup>

<sup>a</sup>School of Mathematics and Statistics, University of St Andrews, St Andrews, UK; <sup>b</sup>IUEM/UBO/LPO, Technopole Brest-Iroise, Plouzané, France

## ABSTRACT

We consider a three-vortex interaction which leads to the vertical alignment of two like-signed quasi-geostrophic vortices in a continuously stratified, rotating fluid. The interaction is close to the classical collapse interaction of three co-planar vortices except that the vortices centres move on close but different horizontal planes. The vertical alignment of vortices helps create larger structures and contributes in physical space to the inverse energy cascade observed in spectral space in geostrophic turbulence.

## ARTICLE HISTORY

Received 9 June 2023  
Accepted 26 July 2023


## KEYWORDS

Quasi-geostrophy; vortex alignment; vortex collapse

## 1. Introduction

Vortices are ubiquitous, key dynamical features in the oceans (Chelton *et al.* 2011). They contribute to a large part of the oceanic transport of mass (Zhang *et al.* 2014), salt and heat (Dong *et al.* 2014). Vortices do not evolve in isolation but interact with other oceanic features such as currents, coasts and bathymetry. They also interact with other vortices. The latter kind of interaction plays an important role in the redistribution of energy across spatial scales. For example, in geostrophic turbulence, energy statistically cascades towards large scales in spectral space (Charney 1971, Nastrom *et al.* 1984). One mechanism put forward to explain in physical space this cascade is the formation of large vortices from the merger of small vortices. Another physical phenomenon which contributes to the increase in size of the vortices is the vertical alignment of vortices. This will be briefly discussed in the following section.

The vertical alignment of two co-rotating vortices was studied in a two-layer system by Polvani (1991). Reinaud and Carton (2020), however, showed that, in a continuously stratified domain, two co-rotating, unit height-to-width aspect ratio, quasi-geostrophic vortices alone do not vertically align in general. This is due to the fact that vortices must undergo strong deformations to vertically align and unit height-to-width aspect ratio vortices are robust. Moreover the conservation of invariants such as the angular impulse and the total energy does not allow the translation required for the two vortices to align when initially horizontally offset. Oblate vortices are more prone to horizontal deformation and may partially vertically align. The vertical alignment remains nonetheless limited in general.

**CONTACT** Jean N. Reinaud  [jean.reinaud@st-andrews.ac.uk](mailto:jean.reinaud@st-andrews.ac.uk), [jnr1@st-andrews.ac.uk](mailto:jnr1@st-andrews.ac.uk)

In this paper, we consider one of the simplest situations where the two co-rotating vortices may, at least temporarily, get closer together horizontally. We then study their potential vertical alignment. We consider a three-vortex interaction where the third vortex rotates in the opposite direction compared to the two co-rotating vortices which may vertically align. The initial conditions derive from the conditions leading to the exact collapse of equivalent point vortices when they lie on the same horizontal plane.

This paper is organised as follows. Section 2 presents the quasi-geostrophic (QG) model used in this study. Section 3 presents the near collapse interactions that lead to the vertical alignment of two co-rotating vortices, using a point vortex model, an ellipsoidal model and the full QG model. We discuss how the parameters of the vortices affect the vertical alignment. We also discuss the limitations of the near collapse interaction to vertically align vortices. Finally, conclusions are presented in section 4.

## 2. The quasi-geostrophic model

The main goal of this paper is to consider the interaction of three finite volume vortices using the QG model in a continuously stratified, rapidly rotating fluid. The QG model is the simplest dynamical model which takes into account the leading-order effects of the background planetary rotation and of the stable density stratification. The QG model is strictly valid for  $Fr^2 \ll Ro \ll 1$ , where  $Fr = U/(NH)$  and  $Ro = U/(fL)$  are the Froude and Rossby number respectively. Here  $U$  is a characteristic horizontal velocity scale for the flow,  $f$  is the Coriolis frequency,  $N$  is the buoyancy frequency and  $L$  and  $H$  are horizontal and vertical characteristic length scales respectively. In an unbounded fluid domain, all flow fields can be derived from a single scalar quantity, the QG potential vorticity anomaly  $q$ , hereinafter referred to as PV for simplicity. The PV,  $q$ , is defined from a stream function  $\varphi$

$$q = \frac{\partial^2 \varphi}{\partial x^2} + \frac{\partial^2 \varphi}{\partial y^2} + \frac{\partial^2 \varphi}{\partial z^2}, \quad (1)$$

where  $z = z_p N/f$ . Here  $x, y, z_p$  are the physical space coordinates,  $z$  is a rescaled vertical coordinate and both  $f$  and  $N$  have been assumed constant. In the absence of diabatic and dissipative effects, the PV,  $q$ , is materially conserved

$$\frac{\partial q}{\partial t} + \mathbf{u} \cdot \nabla q = 0, \quad (2)$$

where

$$\mathbf{u} = \left( -\frac{\partial \varphi}{\partial y}, \frac{\partial \varphi}{\partial x}, 0 \right) \quad (3)$$

is the divergence-free horizontal advecting geostrophic velocity. It should be noted the vertical velocity is not, strictly speaking, zero in the QG model, but it is too small to contribute to the advection of PV in equation (2). Equation (1) can formally be inverted using the appropriate Green's function  $G$

$$\varphi(\mathbf{x}) = \iiint G(\mathbf{x} - \mathbf{x}') q(\mathbf{x}') d^3 \mathbf{x}', \quad (4)$$

where

$$G(\mathbf{x}) = -\frac{1}{4\pi|\mathbf{x}|}. \quad (5)$$

We motivate our study of the vertical alignment of co-rotating vortices by first considering an example of a numerical simulation of QG turbulence. Figure 1 shows a view on the vortex bounding contours for a numerical simulation of QG turbulence. The initial conditions consist of 800 spherical, in the rescaled  $(x, y, z)$ -reference frame, vortices occupying 7% of a triply periodic domain of dimension  $[-\pi, \pi]^3$ . There are 400 vortices with PV  $q = 4\pi$  and 400 vortices  $q = -4\pi$ . All vortices have initially the same volume. The numerical simulation is performed using the Contour Advection Semi-Lagrangian (CASL) algorithm developed first in two dimensions by Dritschel and Ambaum (1997). The PV domain is discretised in the vertical direction using 1024 horizontal layers while the velocity is obtained on a coarser  $256^3$  grid. Equations are marched in time using a fourth-order Runge–Kutta scheme with a time step set by the vortices PV. At  $t = 526$ , we see that some of the largest structures in the flow are the product of the alignment of vortices. We should also point out that part of the increase in size of the vortices is a consequence of vortex merger. The results show the natural occurrence of both vertical alignment and vortex merger in QG turbulence. It is, however, important to point out that there are limitations to the vertical alignment. One cannot create tall columnar vortices from a repeated process of vertical alignments of vortices since such tall columnar vortices are unstable (Dritschel 1996). Nonetheless, two or few vortices may still vertically align and the resulting structure may persist in the flow as far as the height-to-width aspect ratio of the aligned

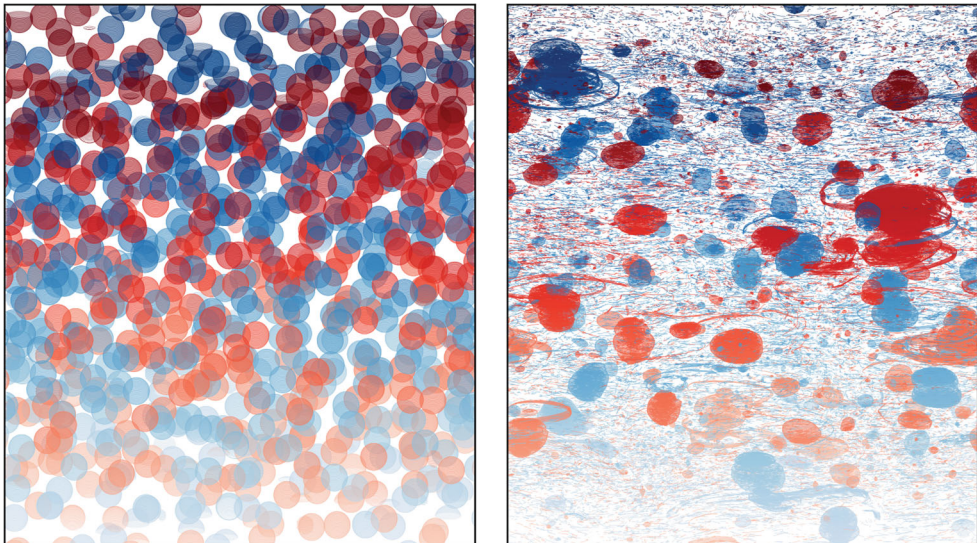


**Figure 1.** Vortex bounding contours on a simulation of quasi-geostrophic turbulence at  $t = 0$  (left) and  $t = 526$  (right). Vortices are viewed orthographically at an angle of  $75^\circ$  degrees from the vertical direction. Cyclonic vortices  $q > 0$  are displayed in red, anticyclonic vortices  $q < 0$  in blue. Colour shading indicates height: dark contours are near the top of the domain, light contour near the bottom.

structure is not too large. Note that Reinaud *et al.* (2003) showed that the most probable vortex height-to-width ratio is 0.83, hence the most vortices are in fact slightly oblate.

### 3. Near collapse interactions

#### 3.1. Point vortices

Before focusing on the interaction of the three finite volume vortices, we start by considering the dynamics of three QG point vortices. Gröbli (1877) showed for the first time the existence of self-similar solutions for the motion of three vortices in two dimensions. These solutions may lead to the finite time collapse of the three vortices to a single point (Aref 1979, Novikov and Sedov 1979, Kimura 1987, Aref 2010). The finite-time collapse solutions were extended to three-dimensional QG dynamics by Reinaud (2021) and further extended to the generalised Euler and QG dynamics by Reinaud *et al.* (2022). The authors showed that these interactions may trigger the merger of the two co-rotating vortices.

For the exact finite time collapse of three QG vortices to a single point, all three vortices must lie on the same horizontal plane  $z = \text{const}$ , due to the lack of vertical advection in QG. Hernández-Garduño and Lacomba (2007) showed that only a self-similar motion can lead to collapse for three vortices in two-dimensional inviscid, incompressible vortex dynamics. We conjecture the same holds for QG vortices due to the formal similarity between the two problems. The existence of a self-similar solution also requires that all three QG vortices lie on the same horizontal plane, as the existence of a time-independent vertical distance between the vortices is inconsistent with the self-similar motion.

It is, however, interesting to note that Jamalooden and Newton (2007) have shown the possibility of the finite-time alignment (collapse) of two opposite-signed point vortices in a three quasi-geostrophic vortex interaction in a two-layer system. In this context, the third vortex does not collapse with the other two vortices.

The initial conditions which lead to the finite-time self-similar collapse of three QG point vortices are given in Reinaud (2021). We denote  $\kappa_i$  the strength of the vortex  $i$ ,  $i \in \{1, 2, 3\}$  and  $\mathbf{X}_i(t) = (X_i(t), Y_i(t), Z_i)$  its time-dependent location. It should be noted that the lack of vertical advection implies that the  $z$ -component of  $\mathbf{x}_i(t)$  is in fact time independent. We denote  $s_i(t)$  the time-dependent length of the side of the triangle formed by the three vortices, opposite to vortex  $i$ , see figure 2. Hence, for example,  $s_3 = |\mathbf{X}_1 - \mathbf{X}_2|$  is the distance between vortices 1 and 2. It should be noted that since all three vortices lie on the same horizontal plane the distances  $s_i$  are horizontal distances. The strength of a QG point vortex is defined as the volume integral of PV over the singular vortex rescaled by  $4\pi$ ,  $\kappa_i = (4\pi)^{-1} \iiint q(\mathbf{x})\delta(\mathbf{X}_i - \mathbf{x})d^3\mathbf{x}$ . Hence, the stream function induced by vortex  $i$  reads

$$\varphi_i(\mathbf{x}) = -\frac{\kappa_i}{|\mathbf{X}_i - \mathbf{x}|}. \quad (6)$$

The conditions for collapse can then be expressed by

$$\frac{\kappa_1\kappa_2}{s_3(0)} + \frac{\kappa_1\kappa_3}{s_2(0)} + \frac{\kappa_2\kappa_3}{s_1(0)} = 0, \quad (7)$$

$$\kappa_1\kappa_2s_3^2(0) + \kappa_1\kappa_3s_2^2(0) + \kappa_2\kappa_3s_1^2(0) = 0. \quad (8)$$

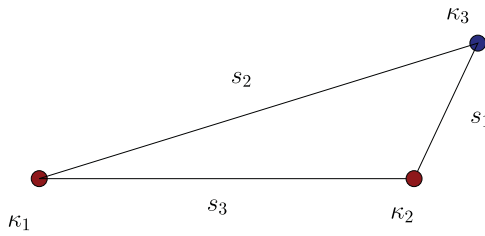


**Figure 2.** Geometry for the collapse of co-planar point vortices (Colour online).

Then the distances between the vortices evolve in a self-similar way

$$s_i(t) = s_i(0)f(t), \quad f(t) = \sqrt[3]{1 - \frac{t}{\tau_c}}, \tag{9}$$

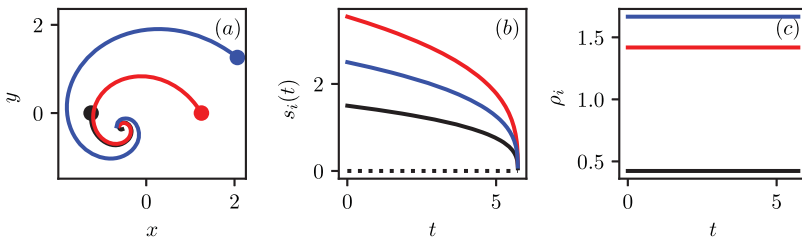
where  $\tau_c$  is the finite collapse time. The detailed derivation of these equations may be found in Reinaud (2021). For example, setting  $s_3(0) = 2.5, \kappa_1 = \kappa_2 = 1$  and  $s_1(0) = 0.6 s_3(0)$  we obtain  $s_2(0) \simeq 1.418 s_3(0)$  and  $\kappa_3 \simeq -0.4216$ . As a diagnostic tool, we define the distance ratios

$$\rho_1 = \frac{s_2}{s_3}, \quad \rho_2 = \frac{s_3}{s_1}, \quad \rho_3 = \frac{s_1}{s_2}. \tag{10}$$

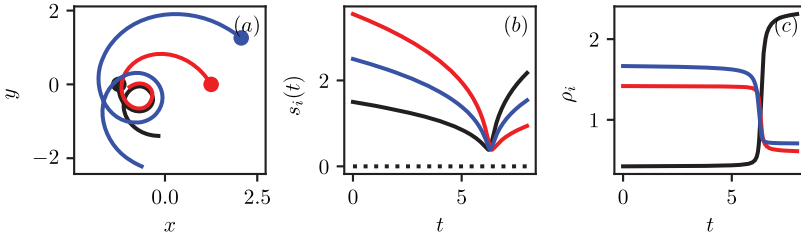
The distance ratios  $\rho_i$  are time independent in a self-similar solution.

Figure 3 shows the three vortex trajectories, the self-similar evolution of the distances  $s_i$  between the vortices and the evolution of the distance ratios  $\rho_i$ . The collapse time  $\tau$  can be analytically predicted, and  $\tau_c \simeq 5.73$ . The results confirm the self-similar motion ( $\rho_i = \text{constant}$ ) where the three vortices inwardly spiral to a single point ( $s_i(\tau_c) = 0$ ).

We next use a near collapse motion to induce the vertical alignment between two co-rotating vortices. To that purpose, we take the same initial conditions as above, but we slightly offset the vertical position of the two co-rotating vortices, here vortices 1 and 2. We first use  $-Z_1 = Z_2 = \delta z$ , while keeping  $Z_3 = 0$ . Although the motion is no longer self-similar and the three point vortices no longer collapse to a single point, the interaction makes the vortices get close together, at least temporarily in the point vortex



**Figure 3.** (a): Top view on the trajectories for the exact collapse of three co-planar point vortices for  $s_3(0) = 2.5, s_1(0)/s_3(0) = 0.6$  and  $\kappa_1/\kappa_2 = 1$  and  $0 \leq t < t_c \simeq 5.73$ . Vortex 1 (black), vortex 2 (red) and vortex 3 (blue). The small solid disks indicate the initial location of the vortices (b): evolution of the horizontal distances between the vortices  $s_i(t), i = \{1, 2, 3\}$  with  $s_1$  in black,  $s_2$  in red and  $s_3$  in blue. (c): Evolution of the ratio  $\rho_i^j$  of the horizontal distances with  $\rho_1$  in black,  $\rho_2$  in red and  $\rho_3$  in blue (Colour online).



**Figure 4.** (a) Top view on the trajectories for the near collapse of three point vortices for  $s_3(0) = 2.5$ ,  $s_1(0)/s_3(0) = 0.6$ ,  $\kappa_1/\kappa_2 = 1$ ,  $z_2 = -z_1 = 0.2$ ,  $z_3 = 0$  and  $0 \leq t < \simeq 7.73$ . (b) Evolution of the horizontal distances between the vortices  $s_i(t)$ ,  $i = \{1, 2, 3\}$ . (c) Evolution of the ratio  $\rho_i^i$  of the horizontal distances. See caption of figure 3 for colours (Colour online).

limit. Results are presented in figure 4 for  $\delta z = 0.2$ . In this case, the vortices are not co-planar and we denote  $s_i$  the horizontal distances between the vortices while  $d_i$  is the full three-dimensional distance,

$$\begin{aligned} s_1 &= ((X_2 - X_3)^2 + (Y_2 - Y_3)^2)^{1/2}, \\ d_1 &= ((X_2 - X_3)^2 + (Y_2 - Y_3)^2 + (Z_2 - Z_3)^2)^{1/2}, \dots \end{aligned} \quad (11)$$

As  $s_i \gg \delta z$ , hence  $d_i \simeq s_i$ , the evolution of  $s_i$  is almost the same as for the exact collapse. The vortices initially get closer together in an almost self-similar way as shown in figure 4. However, as  $s_i$  decreases, the relative departure between  $d_i$  from  $s_i$  increases and the motion departs from the self-similar one. Each horizontal distance  $s_i$  reaches a minimum  $s_i^{m,p}$  at  $t = t_i^{m,p}$ . We have  $s_1^{m,p} \simeq 0.3846$  at  $t_1^{m,p} \simeq 6.24$ ,  $s_2^{m,p} \simeq 0.3846$  at  $t_2^{m,p} = 6.38$ , and  $s_3^{m,p} = 0.3926$  at 6.31. In the point vortex limit, the vortices then separate and have a near self-similar expanding motion. We expect that for finite volume vortices, the initial phase when the vortices get close together can trigger a vertical alignment of the two co-rotating vortices.

### 3.2. Ellipsoidal model

We repeat the same calculation but replacing the point vortices by ellipsoids of uniform PV. We use a simplified dynamical model: the ellipsoidal model developed by Dritschel *et al.* (2003). The ellipsoidal model (ELM) is a Hamiltonian model which filters out high order non-ellipsoidal deformations. It allows to explore a first-order effect of the vortex deformation. Each ellipsoidal vortex is fully described by its PV,  $q_i$ , its centre  $\mathbf{X}_i(t) = (X_i(t), Y_i(t), Z_i)$  and a symmetric  $3 \times 3$ -matrix  $\mathcal{B}_i(t)$  such that the boundary of the ellipsoidal vortex  $i$  is defined by  $(\mathbf{x} - \mathbf{X}_i)\mathcal{B}_i^{-1}(\mathbf{x} - \mathbf{X}_i)^T$ . The evolution of  $\mathbf{X}_i$  and  $\mathcal{B}_i$  is governed by

$$\frac{d\mathbf{X}_i}{dt} = -\frac{1}{\kappa_i} \mathcal{L} \frac{\partial H}{\partial \mathbf{X}_i}, \quad (12)$$

$$\frac{d\mathcal{B}_i}{dt} = \mathcal{S}_i \mathcal{B}_i + \mathcal{B}_i \mathcal{S}_i^T, \quad \text{where } \mathcal{S}_i = -\frac{10}{\kappa_i} \mathcal{L} \frac{\partial H}{\partial \mathcal{B}_i}, \quad (13)$$



and

$$H = \frac{1}{8\pi} \iiint |\nabla\varphi|^2 d^3\mathbf{x}, \quad (14)$$

and  $\kappa_1 = (4\pi)^{-1} \iiint_{V_1} q_i d^3\mathbf{x} = (4\pi)^{-1} q_i V_i = a_x a_y a_z / 3$ .  $V_i$  is the volume of vortex  $i$  and  $a_x$ ,  $a_y$  and  $a_z$  are the semi-axis lengths of the ellipsoidal vortex in the  $x$ ,  $y$  and  $z$ -directions respectively. Finally

$$\mathcal{L} = \begin{pmatrix} 0 & -1 & 0 \\ 1 & 0 & 0 \\ 0 & 0 & 0 \end{pmatrix}. \quad (15)$$

Equations are marched in time with a fourth-order Runge–Kutta scheme and the time step is set by the maximum vortex PV,  $\Delta t = 2\pi / (40 \max\{q\})$ . We use seven singularities to model the external stream function induced each vortices, making it accurate at  $o(d^{-5})$ , where  $d$  is the distance between the vortices centre to the evaluation point, see Dritschel *et al.* (2003) for the details of the method. All three vortices have the same shape initially. We set  $a_x = 0.3017$ ,  $a_y = 0.3$  and  $a_z = 0.2$ . Note that  $a_x$  is chosen to be slightly different from  $a_y$  at  $t = 0$ . This is for numerical reasons and does not introduce any significant dynamical difference from the case  $a_x = a_y$  at  $t = 0$ . Hence the vortices are (near) spheroids of width-to-height aspect ratio  $a_y/a_z = r/h = 1.5$ . The PV of vortices 1 and 2 is set to  $q_1 = q_2 = 2\pi$ . We set  $s_3(0) = 2.5$  and  $s_1(0) = 0.6 s_3(0)$ . The PV of vortex 3 is set to  $q_3 = -0.4216 q_1$ , and we set  $s_2(0) \simeq 1.418 s_3(0)$ , corresponding to the initial conditions for the collapse of the equivalent point vortices used in section 3.1. Here, the strength of vortices 1 and 2,  $\kappa_{1,2} = (4\pi)^{-1} \iiint_{V_{1,2}} q_{1,2} d^3\mathbf{x} = 2\pi a_x a_y a_z / 3 \simeq 0.0379$ . We also have  $\kappa_3/\kappa_1 = q_3/q_1 = -0.4216$ . Similarly to the point vortex simulation, we vertically offset the centres of the two co-rotating vortices,  $Z_2 = -Z_1 \equiv \delta z = a_z = 0.2$  such that the ellipsoidal vortices occupy different but contiguous vertical ranges. We keep  $Z_3 = 0$ . To compare with the point vortex calculation, one can define an advective time scale  $\tau = s_3(0)^3/\kappa_1$ . For the point vortex calculation  $\tau_p = 15.625$  and for the ellipsoid model  $\tau_e \simeq 412.1$  and  $\tau_e/\tau_p \simeq 26.38$ .

We track the centre of each vortex and plot their trajectory as well as the evolution of the distances between the centre of the vortices. Results are shown in figure 5. As for the point vortices, the centres of the ellipsoidal vortices have an inward spiralling, near self-similar motion for  $s_i \gg \delta z$ . The horizontal distances  $s_i$  also reach a minimum  $s_i^{m,e}$ . We have  $s_1^{m,e} = 0.333$  at  $t = t_1^{m,e} = 165.5 \simeq t_1^{m,p} \tau_e/\tau_p$ ,  $s_2^{m,e} = 0.423$  at  $t = t_2^{m,e} = 174 \simeq 6.6 \tau_e/\tau_p$  which is close to  $t = t_2^{m,p} \tau_e/\tau_p = 6.38 \tau_e/\tau_p$ . Finally we have  $s_3^{m,e} = 0.271$  at  $t_3^{m,e} = 170 = 6.43 \tau_e/\tau_p$ . Interestingly the minimum horizontal distance between the two co-rotating vortices  $s_3$  is less for the ellipsoidal vortices than for the point vortices,  $s_3^{m,e} < s_3^{m,p}$ . The shape of the vortices is shown in figure 6 at  $t = 170$ , when  $s_3 = s_3^{m,e}$ . Deformation has helped the two co-rotating vortices get closer together. The two co-rotating vortices also overlap horizontally indicating a partial vertical alignment of their PV as shown in figure 6. Figure 7 shows the evolution of the three semi-axis lengths denoted  $a \leq b \leq c$  for the three ellipsoidal vortices. We have initially  $a_z = a$  and  $a_x = a_y = b = c$ . As the ellipsoidal vortices deform, their principal semi-axis may move. The weaker vortex, vortex 3 with  $|\kappa_3| < \kappa_{1,2}$ , exhibits small amplitude deformation from early times. But overall, vortices deform little until they are close together. Vortices 1 and 2 deform strongly as they start

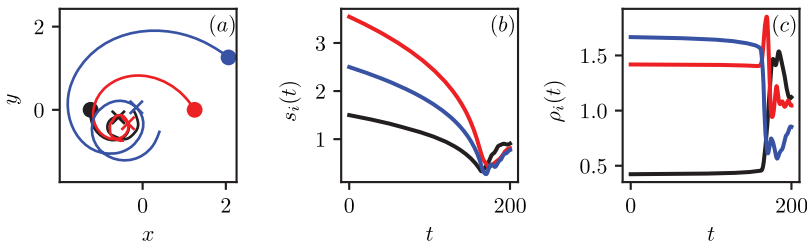


**Figure 5.** (a) Top view on the vortex centres trajectory for ellipsoidal vortices, near collapse of three point vortices for  $s_3(0) = 2.5$ ,  $s_1(0)/s_3(0) = 0.6$ ,  $q_1/q_2 = 2\pi$ ,  $z_2 = -z_1 = 0.2$ ,  $z_3 = 0$  with  $a_x = 0.3017$ ,  $a_y = 0.3$  and  $a_z = 0.2$  at  $t = 0$ . The circles indicate the initial location of the vortex centres. The crosses indicate the location of the vortex centres at  $t = 170$ . (b) Evolution of the horizontal distances between the vortices  $s_i(t)$ ,  $i = \{1, 2, 3\}$ . (c) Evolution of the ratio  $\rho_i^i$  of the horizontal distances. See caption of figure 3 for colours (Colour online).

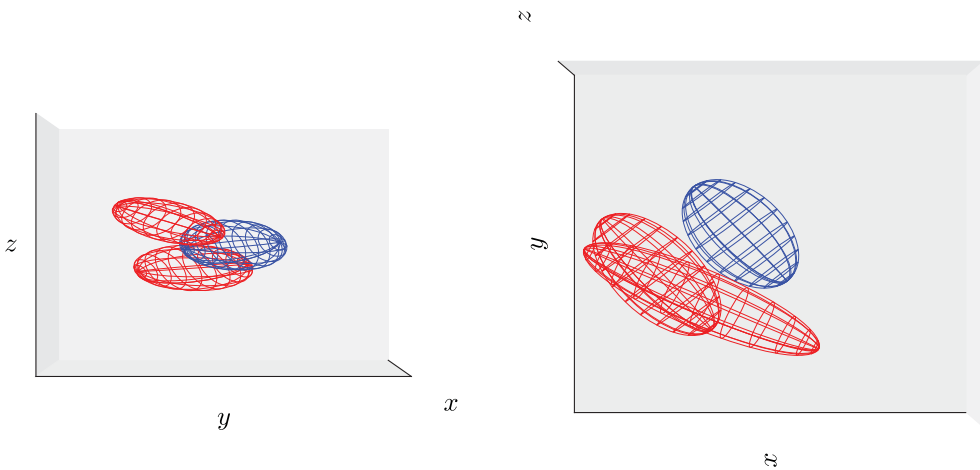


**Figure 6.** Side and top views on the elliptical vortices for  $s_3(0) = 2.5$ ,  $s_1(0)/s_3(0) = 0.6$ ,  $q_1/q_2 = 2\pi$ ,  $z_2 = -z_1 = 0.2$ ,  $z_3 = 0$  with  $a_x = 0.3017$ ,  $a_y = 0.3$  and  $a_z = 0.2$  at  $t = 170$  (corresponding to the crosses in figure 5) (Colour online).

to overlap. The ellipsoidal model does not allow ellipsoidal vortices to split and the vortices retain their volume at all times. At later times, the vortices start to move away from each other. To study the long-term vertical alignment of the co-rotating vortices, we need to consider the full QG dynamics where all vortex deformations, consistent with the QG model, are allowed.

### 3.3. Full QG dynamics

We next consider the evolution of three vortices in the full QG dynamics. We use Contour Surgery (CS) algorithm for three-dimensional QG flow (Dritschel and Saravanan 1994). The method is purely Lagrangian and the fluid domain is unbounded. The full vertical range containing vortices is discretised by 200 horizontal layers. We start by using the same initial conditions as the two examples presented in sections 3.1 and 3.2 but we rescale all distances such that the total height of the domain containing PV is one. This means

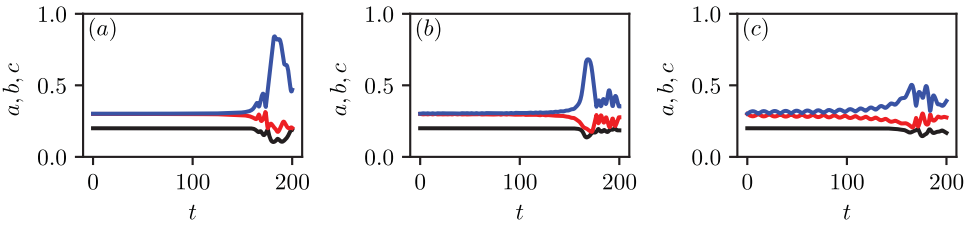


**Figure 7.** Evolution of the three semi-axis lengths for the three ellipsoidal vortices using ELM denoted  $a \leq b \leq c$  for (a) vortex 1, (b) vortex 2, (c) vortex 3 for  $s_3(0) = 2.5, s_1(0)/s_3(0) = 0.6, q_1/q_2 = 2\pi, z_2 = -z_1 = 0.2, z_3 = 0$  with  $a_x = 0.3017, a_y = 0.3$  and  $a_z = 0.2$  (Colour online).

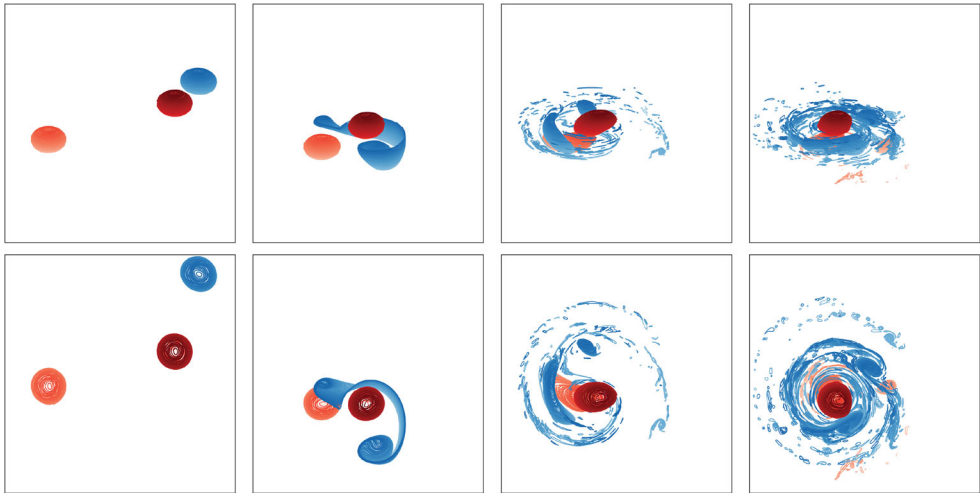


**Figure 8.** Vortices bounding contours for the near collapse of three vortices for case A0a:  $s_3(0) = 3.125, s_1(0)/s_3(0) = 0.6, q_1/q_2 = 2\pi, z_2 = -z_1 = 0.25, z_3 = 0$  with  $a_x = a_y = 0.375$  and  $a_z = 0.25$  at from left to right  $t = 40, 185, 244, 305$ . In the upper row of panels, the vortices are viewed orthographically at an angle of  $65^\circ$  degrees from the vertical direction. In the lower row of panels, the vortices are viewed from the top. Colour shading represents height: darker colour contours are near the top of the domain, lighter colour contours are near the bottom of the domain. Positive PV vortices are seen in shades of red, negative PV vortices are seen in shades of blue. The range  $x \in [-2.5, 2.5]$  is shown (Colour online).

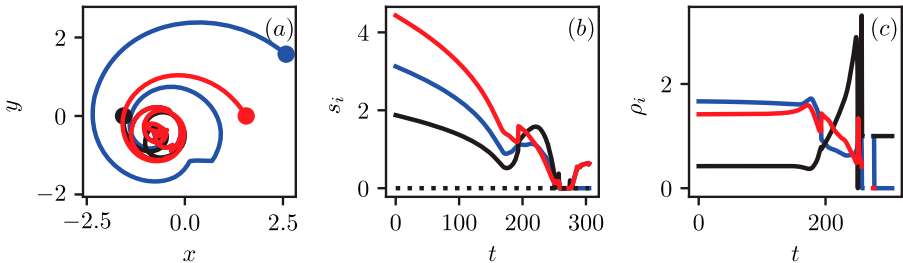


**Figure 9.** (a) Top view on the vortex centres trajectory for QG finite volume vortices near collapse of three point vortices for case A0a:  $s_3(0) = 3.125, s_1(0)/s_3(0) = 0.6, q_1/q_2 = 2\pi, z_2 = -z_1 = 0.25, z_3 = 0$  with  $a_x = 0.375, a_y = 0.375$  and  $a_z = 0.25$  at  $t = 0$ . (b) Evolution of the horizontal distances between the vortices  $s_i(t), i = \{1, 2, 3\}$ . (c) Evolution of the ratio  $\rho_i^j$  of the horizontal distances. See caption of figure 3 for colours (Colour online).

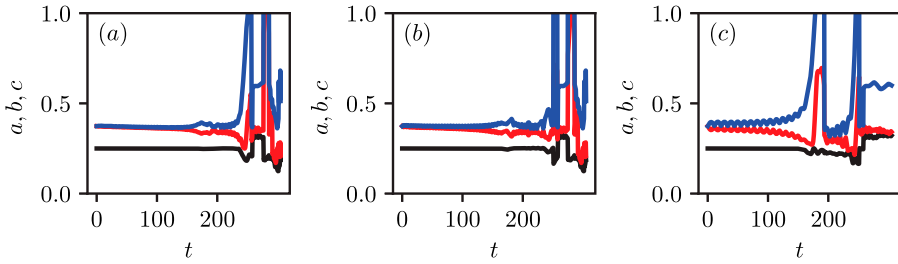


**Figure 10.** Semi-axis lengths for the best-fitted ellipsoid for case  $A0a$ :  $s_3(0) = 3.125$ ,  $s_1(0)/s_3(0) = 0.6$ ,  $q_1/q_2 = 2\pi$ ,  $z_2 = -z_1 = 0.25$ ,  $z_3 = 0$  with  $a_x = 0.375$ ,  $a_y = 0.375$  and  $a_z = 0.25$  at  $t = 0$ . Panel (a) is for vortex 1, panel (b) for vortex 2 and panel (c) for vortex 3 (Colour online).

that all three vortices have an half height  $a_z = 0.25$ , and vortices 1 and 2 are offset vertical such that  $Z_2 = -Z_1 = a_z = 0.25$ . The vortices are initially slightly oblate spheroid of width-to-height aspect ratios  $a_y/a_z = r/h = 1.5$ , hence  $a_x = a_y = 0.375$ . All distances are accordingly rescaled by a factor 1.25 from the cases presented in sections 3.1 and 3.2, and  $s_3(0) = 3.125$ . We keep  $s_2(0) = 0.6 s_3(0)$  and  $q_1 = q_2 = 2\pi$ . This first case is referred to as case  $A0a$ . The advective time scale is  $\tau_q = s_3^2(0)/\kappa_1 = 414.5$  similar to the one of the ellipsoidal case under the scaling,  $\tau_q \sim \tau_e$ . For each vortex, defined as a contiguous region of PV, we define its centre  $\mathbf{X}$  as

$$\mathbf{X} = \frac{\iiint_V \mathbf{x} d^3\mathbf{x}}{\iiint_V d^3\mathbf{x}}, \quad (16)$$

where  $V$  is the vortex (contiguous region of PV) volume. Figure 8 shows the evolution of the vortex bounding contours, from two viewing angles. As the three vortices get closer together, vortex 3, which has the smallest PV in absolute value deforms faster and more than the two co-rotating vortices. A large filament forms from vortex 3 and is entrained by the velocity field induced by vortex 2 and starts to surround vortex 2. A secondary vortex starts to roll up at the end of filament. The central part of the filament thins in the horizontal direction as it is stretched and eventually breaks down into a plethora of smaller filament and PV debris. Meanwhile vortex 2 moves toward vortex 1 and eventually the upper part of vortex 1 is attracted by vortex 2. The upper part of vortex 1 vertically aligns with the lower part of vortex 2. As the vortices continue to swirl, the two co-rotating continue to vertically align while the vortex 3 is mostly destroyed into a large number of small scale secondary structures forming a ring around the aligned co-rotating vortices. The vertical alignment of the two co-rotating structures is also favoured by the ejection of filamentary positive PV and small secondary structures away from the main structure. The figure indicates that some energy has cascaded to larger scale from the alignment while enstrophy has cascades towards small scales via the generation of low energy filaments and debris.

Figure 9 shows the trajectories of the centre of the vortices, the evolution of both the horizontal distances  $s_i$  separating the centre of the vortices and the distance ratios  $\rho_i$ . As in the previous cases, the initial phase of the vortex motion consists in a near self-similar inwardly spiralling motion. The late evolution is more difficult to analyse as the vortices can shed PV and even break into pieces. This makes following individual vortices more ambiguous. The analysis relies on identifying at any time  $t$  the three largest vortices present in the flow. The rapid jumps in the vortex centre trajectories are associated with the splitting

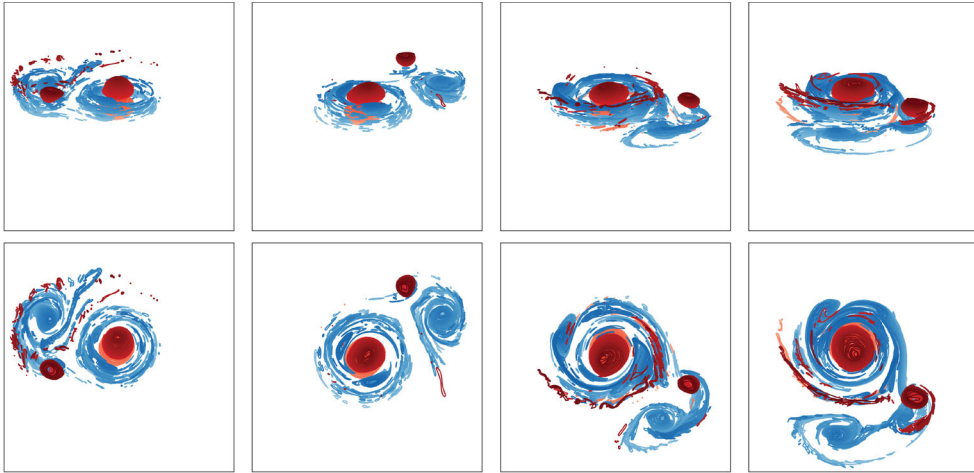


**Figure 11.** Same as figure 8 but from left to right case A1  $a_x = a_y = 0.4375$  at  $t = 224 = 0.7357\tau_{q,A1}$ , case A2  $a_x = a_y = 0.5$  at  $t = 171.5 = 0.7357\tau_{q,A2}$ , case A3  $a_x = a_y = 0.5625$  at  $t = 135.5 = 0.7344\tau_{q,A3}$ , case A4  $a_x = a_y = 0.625$  at  $t = 110 = 0.7373\tau_{q,A4}$ . The range  $x \in [-3.4, 2.2]$  is shown (Colour online).

of the vortices, hence and abrupt change in the position of the centre of the largest part of the vortex. Figure 10 shows the evolution of the three semi-axis lengths  $a \leq b \leq c$  of the ellipsoids best fitted to the three largest vortices in the flow at all times  $t$ . The best fitted ellipsoid to a given vortex is the ellipsoid having the same centre  $\mathbf{X}$  as the vortex and the same second-order geometrical moments

$$M_{ij} = \iiint_V (x^i - X^i)(x^j - X^j)d^3\mathbf{x}, \tag{17}$$

where we have used an index notation  $\mathbf{x} = (x^1, x^2, x^3)$  and  $\mathbf{X} = (X^1, X^2, X^3)$  to simplify the writing. As for the ellipsoidal vortices discussed in section 3.2, the semi-axis lengths for vortex 3 shows early oscillations larger than the ones for vortices 1 and 2, albeit remaining small. The strong deformation of vortex 3 is also clearly captured from  $t \simeq 160$ . This strong deformation makes the trajectory of the vortices further depart from the trajectory of equivalent point vortices. By the end of the simulation, at  $t = 305 = 0.7358\tau_q$ , the largest vortex has volume 1.527 times larger than the initial volume of the vortices.

Keeping the same initial location and the same PV for the three vortices we start by investigating the influence of the vortices width-to-height aspect ratio, first keeping it larger than 1.5. We keep  $a_z = 0.25$  and we set  $a_x = a_y = 0.4375$  (case A1), 0.5 (case A2), 0.5625 (case A3) and 0.625 (case A4) for a vortex width-to-height aspect ratio  $a_y/a_z = r/h = 1.75, 2, 2.25$  and  $2.5$  respectively. The associated advective time  $s_3(0)^2/\kappa_1$  are  $\tau_{q,A1} = 304.5$  for case A1,  $\tau_{q,A2} = 233.1$  for case A2,  $\tau_{1,A3} = 184.2$  for case A3 and  $\tau_{q,A4} = 149.2$  for case A4. Figure 11 shows the vortices for the four additional cases at roughly the same normalised time, corresponding to the end of the simulation. Again, in all cases the two co-rotating vortices have vertically aligned while producing a small secondary satellite vortex and filamentary PV. The relative volume of the largest vortex in the flow at the end of the simulation is reported in table 1. For  $1.5 \leq r/h \leq 2$ , the largest vortex is about 50% larger

**Table 1.** Volume ratio  $V_f/V_i$  of the final volume of the largest vortex to the initial vortex volume for various values of vortex aspect ratios  $r/h$  and the same initial conditions as for figure 11.

Case	A0a	A1	A2	A3	A4
$r/h$	1.5	1.75	2	2.25	2.5
$V_f/V_i$	1.527	1.504	1.536	0.845 / 1.483	0.854 / 1.474

Notes: Figures in *italics* considers the combined volume of the two vertically aligned but disjoint largest co-rotating vortices.

than the initial vortices as a direct consequence of the vertical alignment. For  $r/h > 2$  the situation is slightly different. The two main co-rotating vortices have aligned vertically but, contrarily to the other cases, do not touch. Hence they are identified as two separate coherent structures by the vortex identification algorithm. Each vortex has shed material, with the largest vortex having lost about 15% of its material. However, the combined volume of the two vertically aligned, yet disjoint, structure corresponds to 1.47 times the initial vortex volume, comparable to the other cases for  $r/h \leq 2$ .

We also verify that the vertical alignment of moderately oblate vortices is a generic feature of a near collapse interaction by investigating the interaction under other initial conditions. In the next examples, we keep the same vortices 1 and 2 but we set  $s_1(0) = |\mathbf{X}_2 - \mathbf{X}_3| = 0.7 s_3(0)$  instead. The PV of vortex 3,  $q_3 = -0.3841$ , corresponding to the strength required for the self-similar collapse of three co-planar point vortices. The distance  $s_2(0) = 1.3056 s_3(0)$ . As in the previous case the vortices are vertically offset,  $-Z_1 = Z_2 = \delta_z = a_z = 0.25$  and  $Z_3 = 0$ . This case is referred to as case B0. Results are presented in figure 12. Similar results are presented for  $s_1(0) = |\mathbf{X}_2 - \mathbf{X}_3| = 0.8 s_3(0)$  (case C0) in figure 13. In this case,  $q_3 = -0.48017 q_1$  and  $s_2(0) = 1.2011 s_3(0)$ . In both cases, the near collapse interaction induces the vertical alignment of the two co-rotating vortices while the opposite-signed vortex, vortex 3 is partially destroyed and shed many debris and filaments which swirl around the aligned structure.

In all the examples above the two co-rotating vortices, vortices 1 and 2, have the same strength. We next consider the near collapse interaction of the three vortices when the two co-rotating vortices have unequal strength. Since the vortices have uniform PV, their strength is simply the product of their PV and their volume. Hence we can modify the strength of a vortex by modifying its volume or its PV (or both). In the first three numerical experiments, we keep the volume of all three vortices the same, and we change the PV of vortex 2. Recall that the initial conditions used in these numerical experiments derive from the condition for the exact collapse of the equivalent co-planar point vortices. These conditions depend on the strength ratio of the two like-signed vortices. Hence the initial location and the PV of vortex 3 depends on the PV of vortex 2, even when the other parameters are fixed.

Figures 14–16 show the results for  $s_3(0) = 3.125$ ,  $s_1(0)/s_3(0) = 0.7$ ,  $Z_2 = -Z_1 = 0.25$ ,  $Z_3 = 0$  with  $a_x = a_y = 0.375$ ,  $a_z = 0.25$  and  $q_2/q_1 = 0.7$  (case B1), 0.5 (case B2a) and 0.3 (case B3) respectively. The other parameters, determined by the collapse conditions for equivalent co-planar vortices are as follows. For case B1 we have  $q_3 = -0.3228 q_1$  and  $s_2(0) = 1.3512 s_1(0)$ . For case B2,  $q_3 = -0.2323 q_1$  and  $s_2(0) = 1.3812 s_3(0)$ . Finally for case B3,  $q_3 = -0.14036 q_1$  and  $s_2(0) = 1.4108 s_3(0)$ . As the PV of vortex 2 is reduced, the deformation of vortex 2 increases. For  $q_2/q_1 = 0.7$  and 0.5 the interaction is qualitatively

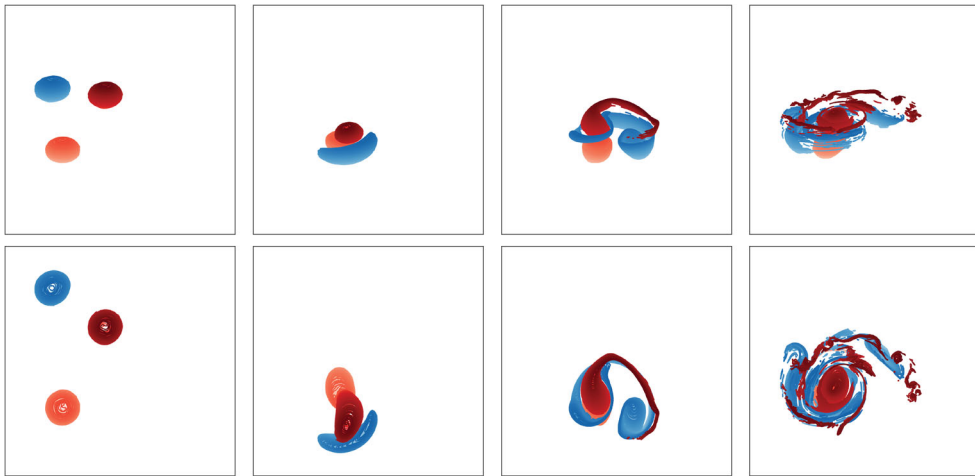


**Figure 12.** Vortices bounding contours for the near collapse of three vortices for case B0:  $s_3(0) = 3.125$ ,  $s_1(0)/s_3(0) = 0.7$ ,  $q_1 = q_2 = 2\pi$ ,  $Z_2 = -Z_1 = 0.25$ ,  $Z_3 = 0$  with  $a_x = a_y = 0.375$  and  $a_z = 0.25$  at  $t = 140, 200, 210$  and  $236.5$ . In the lower row of panels, the vortices are viewed from the top. Colour shading represents height: darker colour contours are near the top of the domain, lighter colour contours are near the bottom of the domain. Positive PV vortices are seen in shades of red, negative PV vortices are seen in shades of blue. The domain  $x \in [-2.5, 2.5]$  is shown (Colour online).

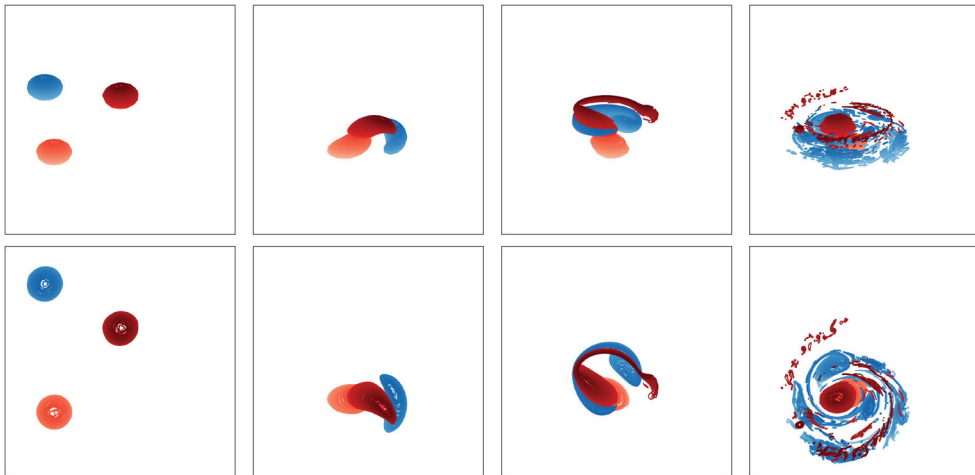


**Figure 13.** Vortices bounding contours for the near collapse of three point vortices for case C0:  $s_3(0) = 3.125$ ,  $s_1(0)/s_3(0) = 0.8$ ,  $q_1 = q_2 = 2\pi$ ,  $Z_2 = -Z_1 = 0.25$ ,  $Z_3 = 0$  with  $a_x = a_y = 0.375$  and  $a_z = 0.25$  at  $t = 165, 305, 312.5$  and  $375$ . Colours and viewing angles are the same as in figure 12. The domain  $x \in [-2.5, 2.5]$  is shown (Colour online).

similar to the previous case with  $q_2 = q_1$ . A large part of vortex 2 vertically aligns with vortex 1. For  $q_2/q_1 = 0.3$ , the situation is slightly different. As before a large tongue of PV from vortex 2 moves toward vortex 1. The tongue of PV is entrained by the rotation induced by vortex 1 and is stretched. But instead of forming a compact vortex vertically aligned with vortex 1, it curls around vortex 1. The tongue eventually reconnects on itself to form a

torus of PV vertically aligned with vortex 1. This is reminiscent of the binary interaction of two co-rotating vortices of very different PV explored in Özügürü *et al.* (2008). Indeed, in such cases, instead of merging, the vortex with the small PV is partially strained out and sheds a large tongue of PV that eventually forms a ring around the large PV vortex. This is due to the reduced ability of the tongue of PV from low PV vortex to withstand the strain and shear induced by the other vortex (figure 17). In the next set of numerical experiments, we change the overall strength of a vortex by changing its volume. We revisit the case *B2a* described above with  $s_3(0) = 3.125$ ,  $s_1(0)/s_3(0) = 0.7$ ,  $Z_2 = -Z_1 = 0.25$ ,  $Z_3 = 0$  with  $a_x = a_y = 0.375$ ,  $a_z = 0.25$  and  $\kappa_1 = 2\kappa_2$ , but keeping  $q_1 = q_2 = 2\pi$ . This means the volume of vortex 2 is half the volume of vortex 1. For simplicity, vortex 2 has same width-to-height ratio set to  $r/h = a_x/a_z = 1.5$  as vortex 1. In the first experiment, vortex 3 has the same volume as vortex 1 (case *B2b*). Then, in a following numerical experiment, we keep the same parameters as case *B2b* except that we increase the width-to-height ratios of all three vortices to  $r/h = a_x/a_z = 2$  (case *B4a*). Finally in the third experiment we use the same set-up as case *B4a* but let  $q_3 = -q_1 = -q_2 = -2\pi$  and we reduce the volume of vortex 3 to keep the same strength (case *B4b*).

Results are presented in figure 12. We first compare cases *B2a* from figure 15 and *B2b* from figure 12. The early evolution (not shown) is very similar between the two cases. In case *B2a* vortex 2 has a larger volume than in case *B2b*. Hence as it approaches vortex 1, the minimum distance between the edges of the vortices 1 and 2 is smaller in case *B2a* than in *B2b* for an overall similar trajectory. In case *B2a* the main first deformation is the deformation of the low PV vortex 2 which leads to the vertically alignment of some of the PV of vortex 2 with vortex 1. This weakens the interaction of vortex 2 with the opposite-signed vortex 3 as PV from vortex 2 migrates towards vortex 1 and away from vortex 3. Hence vortex 3 remains compact. On the contrary, in case *B2b*, vortex 2 has a larger PV than in case *B2a* and its edge is also further away from the edges of vortex 1. The deformation of

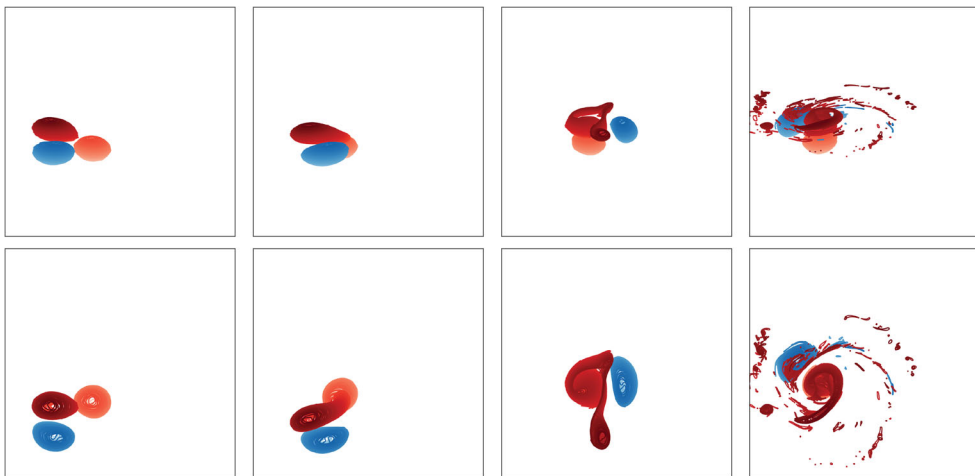


**Figure 14.** Vortices bounding contours for the near collapse of three point vortices for case *B1*:  $s_3(0) = 3.125$ ,  $s_1(0)/s_3(0) = 0.7$ ,  $q_1 = 2\pi$ ,  $q_2 = 0.7q_1$ ,  $Z_2 = -Z_1 = 0.25$ ,  $Z_3 = 0$  with  $a_x = a_y = 0.375$  and  $a_z = 0.25$  at  $t = 246, 250, 513$  and  $362.5$ . Colours and viewing angles are the same as in figure 12. The domain  $x \in [-2.5, 2.5]$  is shown (Colour online).



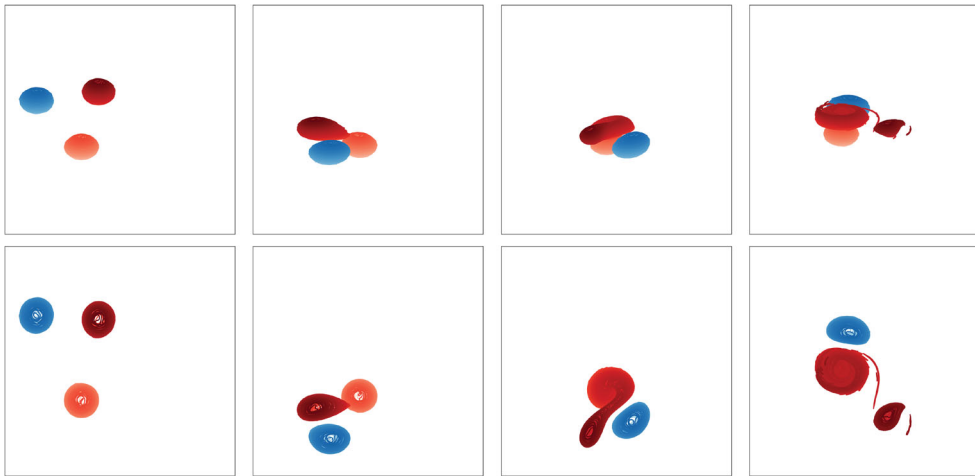


**Figure 15.** Vortices bounding contours for the near collapse of three point vortices for case  $B2a$ :  $s_3(0) = 3.125$ ,  $s_1(0)/s_3(0) = 0.7$ ,  $q_1 = 2\pi$ ,  $q_2 = 0.5 q_1$ ,  $Z_2 = -Z_1 = 0.25$ ,  $Z_3 = 0$  with  $a_x = a_y = 0.375$  and  $a_z = 0.25$  at  $t = 250, 322.5, 335$  and  $360$ . Colours and viewing angles are the same as in figure 12. The domain  $x \in [-3.1, 1.9]$  is shown (Colour online).

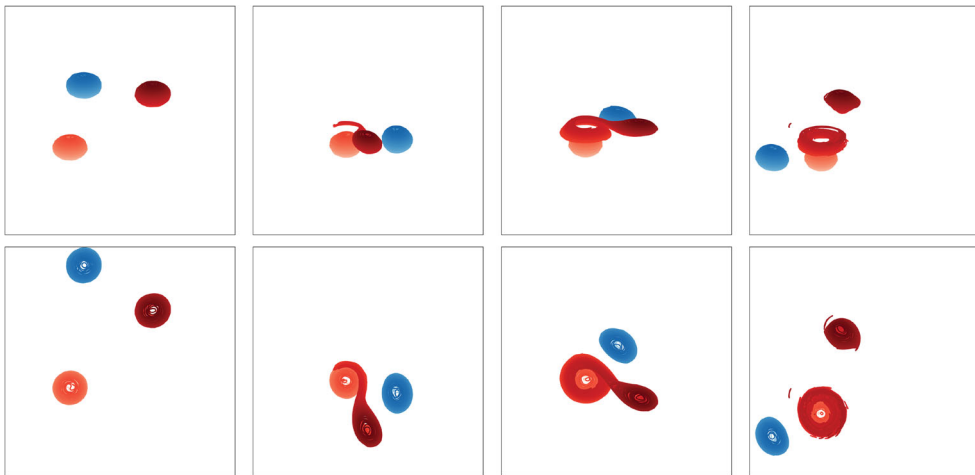


**Figure 16.** Vortices bounding contours for the near collapse of three point vortices for case  $B3$ :  $s_3(0) = 3.125$ ,  $s_1(0)/s_3(0) = 0.7$ ,  $q_1 = 2\pi$ ,  $q_2 = 0.3 q_1$ ,  $z_2 = -z_1 = 0.25$ ,  $z_3 = 0$  with  $a_x = a_y = 0.375$  and  $a_z = 0.25$ . Colours and viewing angles are the same as in figure 12. The domain  $x \in [-3.1, 1.9]$  is shown (Colour online).

vortex 2 towards vortex 1 is less pronounced. The interaction between vortices 1 and 2 with vortex 3 leads to the straining of vortex 3. Eventually vortex 2 vertically aligns with vortex 1 as it becomes sufficiently close to vortex 1, at later stage compared to case  $B2a$ . Meanwhile vortex 3 gets further strained around the aligned vortex. As expected the ability of vortices to deform when subjected to the strain and shear induced by the other vortices is a key factor in the complex nonlinear evolution of the vortices. Case  $B4a$  is qualitatively similar to case  $B2b$ . The evolution of  $B4b$  is, however, qualitatively different. Here, vortex 3 is smaller

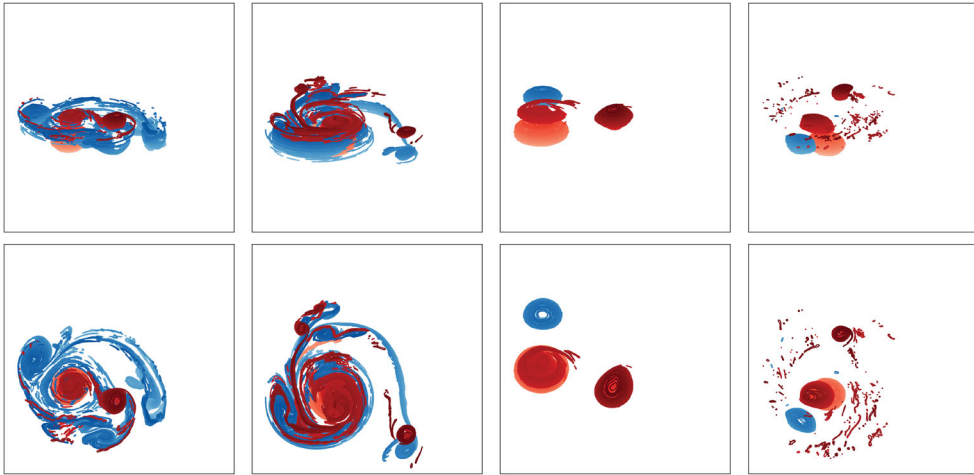


**Figure 17.** Vortex bounding contours for, from left to right, case *B2b* at  $t = 360$  showing  $x \in [-2.8, 2.2]$ , case *B4a* at  $t = 205$  showing  $x \in [-3.1, 1.9]$ , case *B4b* at  $t = 250$  showing  $x \in [-2.5, 2.5]$  and case *A0b* at  $t = 305$   $x \in [-2.5, 2.5]$ . Colours and viewing angles are the same as in figure 12 (Colour online).

with a larger PV compared to case *B4a*. As a consequence, vortex 3 is less prone to deformation and remains compact. As vortex 3 retains more of its material it remains stronger in the interaction, which in turns weakens the interaction between vortices 1 and 2. Recall that only the size and PV of vortex 3 differ between the two cases (while its strength remains the same). In case *B4b*, a smaller part of vortex 2 has vertically aligned with vortex 1. For example at  $t = 205$  vortex 1 has a volume  $V_1(t = 360) = 0.944 V_1(t = 0)$  for case *B4a*, which is comparable to  $V_1(t = 360)/V_1(t = 0) = 0.922$  in case *B4b*. Vortex 1 vertically aligns with a portion of vortex 2 of volume  $V_{a,2}(t = 360) = 0.388 V_2(t = 0)$  in case *B4a* while it is only  $V_{a,2}(t = 360) = 0.1613 V_2(t = 0)$  in case *B4b*. The alignment of vortices 1 and 2 is favoured when vortex 3 is eventually weakened (strained out), after having played its role in the near collapse interaction and made vortices 1 and 2 close together.

Finally we revisit case *A0a* by setting  $q_3 = -q_1 = -2\pi$  and changing its volume to maintain  $\kappa_3 = -0.4216\kappa_1$ . This case is referred to as *A0b* and is shown in figure 12. Again, the main first difference between the two cases is the fate of vortex 3. The low PV/large volume vortex 3 of case *A0a* is strained out while the large PV/small volume vortex 3 of case *A0b* remains compact. At  $t = 305$ , however  $V_f/V_i = 1.490$  for case *A0b* which is only marginally smaller than for the case *A0a* at the same time with  $V_f/V_i = 1.504$  as reported in table 1. In this case, the two co-rotating vortices are initially identical and the *late* evolution of the counter-rotating vortex 3 has less influence on the vertical alignment of vortices 1 and 2.

In the numerical experiments of near collapse interactions described above, the interactions resulted in a partial alignment of the two co-rotating vortices. Results show that the ability of the vortices to deform is central to the alignment. For a given vortex strength, large volume, low PV vortices are more likely to deform. The vortex width-to-height aspect ratio also plays a role on the vortices' ability to deform. In the numerical experiments above, we have focused on oblate vortices with a width-to-height aspect ratio of 1.5 and above. In

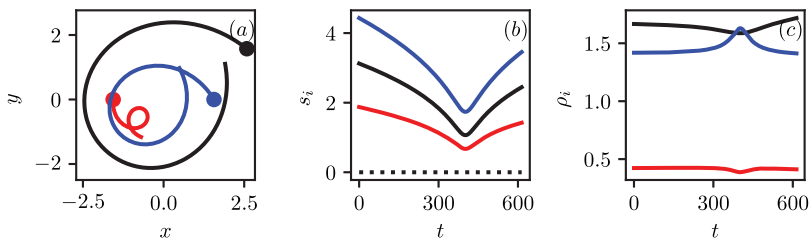


**Figure 18.** (a) Top view on the vortex centres trajectory for QG finite volume vortices near collapse of three point vortices for case A5:  $s_3(0) = 3.125$ ,  $s_1(0)/s_3(0) = 0.6$ ,  $q_1/q_2 = 2\pi$ ,  $z_2 = -z_1 = 0.25$ ,  $z_3 = 0$  with  $a_x = a_y = a_z = 0.25$  at  $t = 0$ . (b) Evolution of the horizontal distances between the vortices  $s_i(t)$ ,  $i = \{1, 2, 3\}$ . (c) Evolution of the ratio  $\rho_i^j$  of the horizontal distances. See caption of figure 3 for colours (Colour online).

the next section, we discuss some limitations of the near collapse interaction to trigger the vertical alignment of the two co-rotating vortices.

### 3.4. Less oblate vortices

We first revisit the case A0a but changing the width of the vortices. We first set  $a_x = a_y = a_z = 0.25$  keeping all the other parameters the same as case A0a. We denote this case A5 and the vortices are spherical  $r/h = 1$ . We also consider the same interaction but with  $a_x = a_y = a_z = 0.3125$  corresponding to  $r/h = 1.25$  (case A6). In both cases, the vortices are more less oblate than in case A0a and they deform less. As a consequence, the two co-rotating vortices do not vertically align. Results are shown in figure 18 for case A5 and in figure 19 for case A6. As in the previous cases the vortices start by spiralling inwardly, see panels (a) of figures 18 and 19. The early motion of the vortices is nearly self-similar, as shown in the panels (c) of both figures. All three horizontal distances  $s_i$  between the vortices reach a minimum before increasing again. Then the late evolution follows a near self-similar expanding motion. One of the main differences between the trajectories of the vortices and the ones of equivalent point vortices is the significant difference between the values of three minimum distances  $s_i^{\min}$  for the finite volume vortices. The lack of alignment and the eventual expanding motion suggests that the vortices need to be relatively oblate to deform enough for the alignment to occur.

### 3.5. Influence of the vertical offset $\delta z$

In the previous numerical experiments, the two co-rotating vortices are vertically offset such that they occupy contiguous regions in the vertical direction, i.e.  $\delta z = a_z$ . Hence the vortices may align on the top of one another to create a single region of contiguous PV, as seen for example in cases A0a, A1 and A2. We have, however, seen that the interaction may erode the bottom of vortex 2 (the upper vortex in the co-rotating pair) and/or the top of vortex 1 (the lower vortex in the vortex pair). In that case, the vortices may still eventually vertically align even if there is a small vertical gap with no PV between

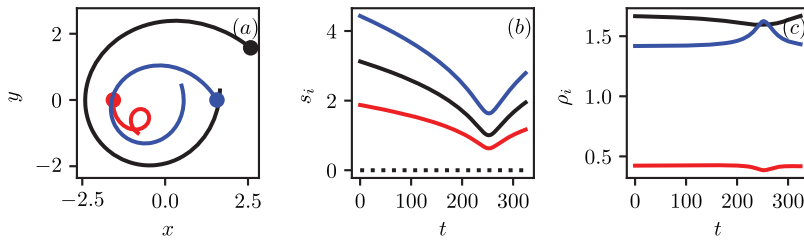


**Figure 19.** (a) Top view on the vortex centres trajectory for QG finite volume vortices near collapse of three point vortices for case A6:  $s_3(0) = 3.125$ ,  $s_1(0)/s_3(0) = 0.6$ ,  $q_1/q_2 = 2\pi$ ,  $z_2 = -z_1 = 0.25$ ,  $z_3 = 0$  with  $a_x = a_y = 0.3125$  and  $a_z = 0.25$  at  $t = 0$ . (b) Evolution of the horizontal distances between the vortices  $s_i(t)$ ,  $i = \{1, 2, 3\}$ . (c) Evolution of the ratio  $\rho_i^j$  of the horizontal distances. See caption of figure 3 for colours (Colour online).

**Table 2.** Case reference and indication of the outcome of the interaction for the three vortices for  $s_3(0) = 3.125$ ,  $s_1(0)/s_3(0) = 0.6$ ,  $q_1 = q_2$  and  $a_z = 0.2$  and various values of  $a_x = a - y = r_h$  and  $\delta z$ .

$r_h$	0.375	0.5	0.625	0.75
$\delta z = 0.3125$	case D0a: N	case D1a: A	case D2a A	case D3a A
$\delta z = 0.375$	case D0b: N	case D1b: N	case D2b P	case D3b: A

Notes: *N* means no alignment. *A* means alignment. *P* means partial alignment.

the two aligned co-rotating vortices. It is therefore interesting to investigate the possibility for the two co-rotating vortices to vertically align when  $\delta z > a_z$  at  $t = 0$ . We run two new sets of numerical experiments. In both sets, we use the same basic set-up with  $s_3(0) = 3.125$ ,  $s_1(0)/s_3(0) = 0.6$ ,  $\kappa_1 = \kappa_2$  as in case A0a. In all cases, we set  $a_z = 0.25$  and we vary  $a_x = a_y = r_h = 0.375, 0.5, 0.625, 0.75$  for two values of  $\delta z = 0.3125$  and  $0.375$ . The third, counter-rotating vortices remains at  $Z_3 = 0$ . Results are first summarised in the table 2. Increasing the vertical offset  $\delta z$  makes the initial condition further from the exact collapse conditions. It also weakens the interaction between the two co-rotating vortices as they never can get closer than the non-zero vertical gap between them. On the other hand, as seen before, increasing the width of the vortices favours the alignment. Results show that, as expected alignment, is favoured by small  $\delta z$  and large  $r_h$ . Examples of such alignment are presented in figure 20 for case D1a with  $(r_h, \delta z) = (0.5, 0.3125)$ , D2a with  $(0.625, 0.3125)$ , D3a with  $(0.75, 0.3125)$  and D3b with  $(0.75, 0.375)$ . For case D0a with  $(r_h, \delta z) = (0.375, 0.3125)$ , D0b with  $(0.375, 0.375)$  and D1b with  $(0.5, 0.375)$  the two co-rotating do not vertically align and the trajectories of the vortices centres (not shown) resembles the one of cases A5 or A6 shown in figures 18 and 19. Another, new intermediate regime is observed for case D2b with  $r_h = 0.625$  and  $\delta z = 0.375$ , where the two co-rotating vortices nearly align and the third counter rotating remains nearby the co-rotating pair. The horizontal distances  $s_i$  between the three vortices oscillate slightly but remain roughly comparable through time. The evolution of the vortex trajectories, distances  $s_i$  and distance ratios  $\rho_i$  is presented in figure 21 for that case. Top views on the vortex bounding contours are presented in figure 22.

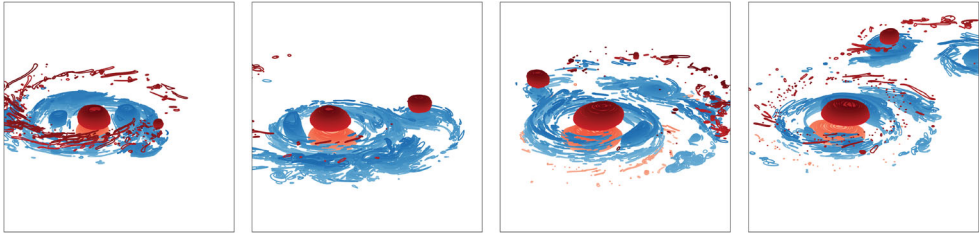


**Figure 20.** Vortices bounding contours for the near collapse of three point vortices for, from left to right case  $D1a$  at  $t = 512$ ,  $D2a$  at  $t = 363$ ,  $D3a$  at  $t = 212$  and case  $D3b$  at  $t = 461$ . Colours and viewing angles are the same as in figure 12 (Colour online).

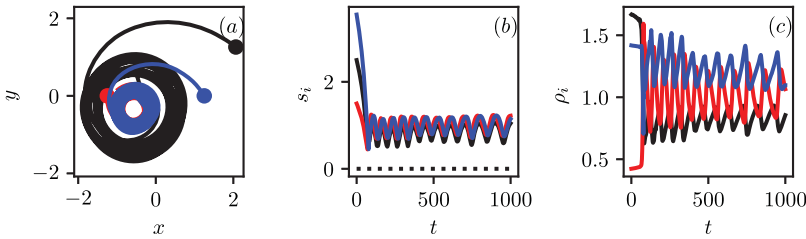


**Figure 21.** (a) Top view on the vortex centres trajectory for QG finite volume vortices near collapse of three point vortices for case  $D2b$  with  $s_3(0) = 3.125$ ,  $s_1(0)/s_3(0) = 0.6$ ,  $q_1/q_2 = 2\pi$ ,  $Z_2 = -Z_1 = 0.375$ ,  $Z_3 = 0$  with  $r_h = 0.625$ ,  $a_z = 0.25$  at  $t = 0$ . (b) Evolution of the horizontal distances between the vortices  $s_i(t)$ ,  $i = \{1, 2, 3\}$ . (c) Evolution of the ratio  $\rho_i$  of the horizontal distances. See caption of figure 3 for colours. (Colour online).

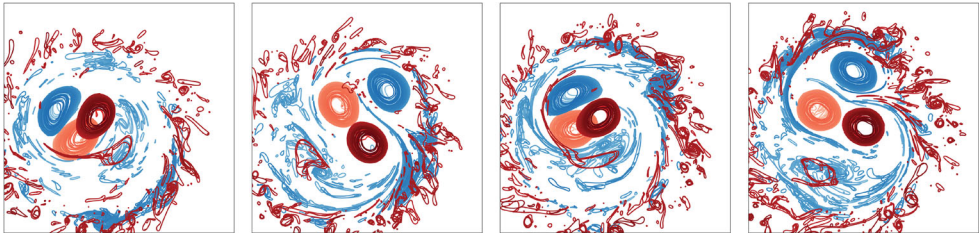


**Figure 22.** Top view on the vortex bounding contour for case  $D2b$  with  $s_3(0) = 3.125$ ,  $s_1(0)/s_3(0) = 0.6$ ,  $q_1/q_2 = 2\pi$ ,  $Z_2 = -Z_1 = 0.375$ ,  $Z_3 = 0$  with  $r_h = 0.625$ ,  $a_z = 0.25$  at from left to right  $t = 850$ ,  $886$ ,  $955$  and  $1000$  (Colour online).

### 3.6. Influence of the shape of the vortices

We finally consider the influence of the initial geometrical shape of the vortices. In the previous numerical experiments, the vortices were initially ellipsoidal. Vortices 1 and 2 are occupying contiguous yet different heights. Hence here is little volume of PV in the range of height where the vortices 1 and 2 are close together in the vertical direction. Hence, we next consider the interaction of cylindrical vortices, increasing the volume of PV in the vertical the range of heights where the vortices potentially align. We expect this choice to favour the vertical alignment of the two co-rotating vortices.

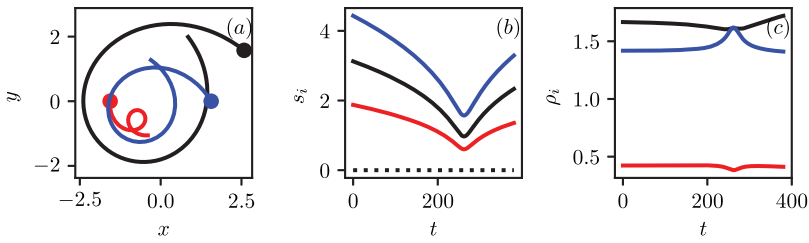


**Figure 23.** (a) Top view on the vortex centres trajectory for QG finite volume vortices near collapse of three point vortices for case  $E0$ :  $s_3(0) = 3.125$ ,  $s_1(0)/s_3(0) = 0.6$ ,  $q_1/q_2 = 2\pi$ ,  $Z_2 = -Z_1 = 0.25$ ,  $Z_3 = 0$  with  $D = 0.5$ ,  $H = 0.5$  at  $t = 0$ . (b) Evolution of the horizontal distances between the vortices  $s_i(t)$ ,  $i = \{1, 2, 3\}$ . (c) Evolution of the ratio  $\rho_i^j$  of the horizontal distances. See caption of figure 3 for colours (Colour online).

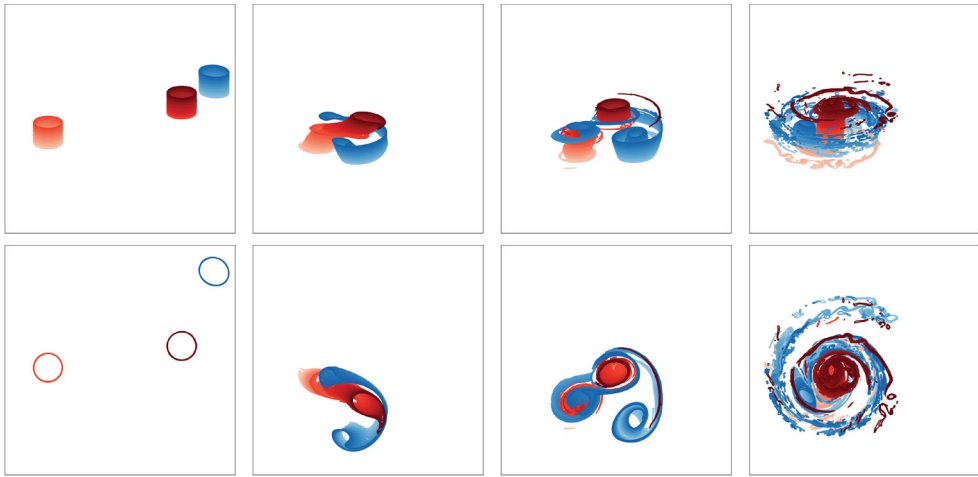


**Figure 24.** Vortices bounding contours for the near collapse of three vortices for case  $E1$ :  $s_3(0) = 2.5$ ,  $s_1(0)/s_3(0) = 0.6$ ,  $q_1 = 2q_2 = 2\pi$ ,  $z_2 = -z_1 = 0.2$ ,  $z_3 = 0$  with  $r_h = 0.25$  and  $h = 0.2$ , at  $t = 25, 171, 180$  and  $241$ . Colours and viewing angles are the same as in figure 12 (Colour online).

Figure 23 shows the results for  $s_3(0) = 3.125$ ,  $s_1(0) = 0.6 s_3(0)$ ,  $q_1 = q_2 = 2\pi$ . All three vortices are initially a cylinder of uniform PV of diameter  $D = 0.5$  and height  $H = 0.5$  centred at  $-Z_1 = Z_2 = H/2 = 0.25$  and  $Z_3 = 0$ . The other parameters are the same as for case  $A0a$  with  $q_3/q_1 = -0.4216$  and  $s_2(0) \simeq 1.418 s_3(0)$ . We refer to this case as case  $E0$ . As for the case for spherical vortices (case  $A5$ ), the vortices do not deform enough nor the two co-rotating vortices ever become close enough to vertically align. The trajectory of the vortex centres, the evolution of the horizontal distances between the vortices and their ratios are similar to the ones for the spherical vortices shown in figure 18. Increasing the vortices diameter to  $D = 0.625$  (case  $E1$ ) and  $D = 0.75$  (case  $E2$ ) while keeping the other parameters the same as case  $E0$  triggers the vertical alignment of the two co-rotating vortices. It should be noted that the vortex width-to-height ratio, the vortex centre locations and the vortex strength ratios of case  $E1$  are the same as the one of case  $A6$ . The only difference is the initial geometrical shape of the vortices. The co-rotating vortices align in  $E1$  and do not align in  $A6$ . Hence, as expected, the increase of the PV volume available

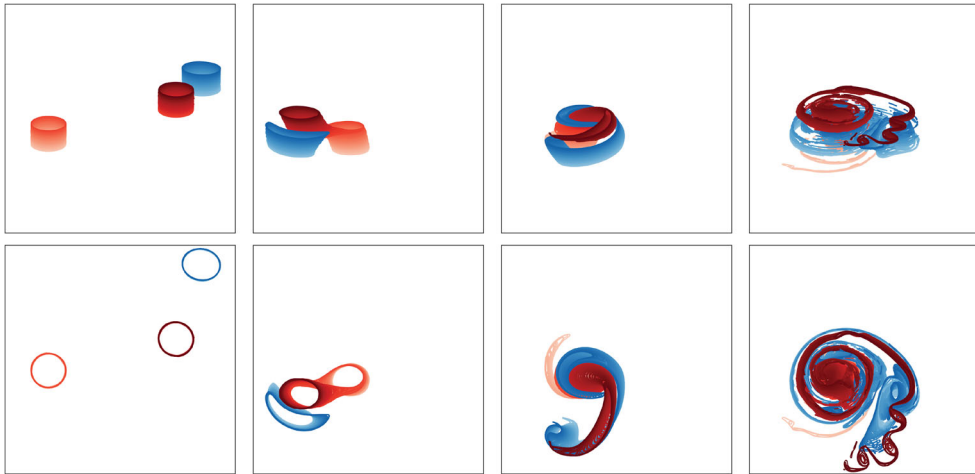


**Figure 25.** Vortices bounding contours for the near collapse of three vortices for case  $E2$ :  $s_3(0) = 2.5$ ,  $s_1(0)/s_3(0) = 0.6$ ,  $q_1 = 2q_2 = 2\pi$ ,  $z_2 = -z_1 = 0.2$ ,  $z_3 = 0$  with  $r_h = 0.3$  and  $h = 0.2$ , at  $t = 25, 109, 117.5$  and  $144$ . Colours and viewing angles are the same as in figure 12 (Colour online).

in the region where vortices 1 and 2 can align increase the vortices ability to align. The overall efficiency of the alignment is, however, similar to the cases with ellipsoidal vortices with the ratio of the volume of the largest vortex in the flow  $V_f$  to the initial vortex volume  $V_i$  is  $V_f/V_i = 1.55$  for case  $E1$  at  $t = 241$ , and it is  $V_f/V_i = 1.46$  for case  $E2$  at  $t = 144$  (figures 24 and 25).

#### 4. Conclusion

In this paper, we have studied the vertical alignment of two co-rotating vortices. The alignment is triggered by a near collapse interaction between three vortices. The condition for the near collapse interaction derives from the condition of exact collapse for three co-planar point vortices. For finite volume vortices, the vertical alignment of the two co-rotating vortices relies on the deformation of the vortices as they approach each other. In our numerical experiments, we have shown that oblate vortices can get close enough during the interaction to undergo the necessary deformation to trigger the vertical alignment of the two co-rotating vortices. More compact vortices may not align because they do not get close enough or do not deform enough to align. In the case the vortices align, the largest vortex forms either as a single contiguous structure or a compound structure consisting of two neighbouring, vertically aligned structures. The resulting structure is about 50% larger than the initial vortices for equal PV and equal volume co-rotating vortices. This provides an efficient route for an upscale cascade of energy in physical space. As for the binary merger interactions of two vortices, the alignment of different size and/or strength vortices is typically less efficient. Meanwhile we often see a plethora of filaments, small debris and secondary satellite vortices surrounding the aligned structure. These feed a direct cascade of enstrophy. In particular, the main aligned structure is often surrounded by opposite-signed PV coming from the third counter-rotating vortex which has been partially strained out. This situation is increasingly observed in high-resolution realistic simulation in basin

using the primitive equations (Aguiar *et al.* 2013, D'Addezio *et al.* 2020, Gula *et al.* 2016). For a moderately increased vertical offset, we also observed a case where all three vortices remain in close proximity. All these configurations of vortices are reminiscent of what can be observed in areas of vortex formation such as the Gulf of Cadiz (Ambar *et al.* 2008, Quentel *et al.* 2011) where multiple vortices coexist in the same area. Finally when the vortices cannot align because they do not deform enough during the phase of the evolution when they are at their closest, the vortices separate continue moving apart from each other in a near self-similar way, transporting their properties away over long distances.

## Disclosure statement

No potential conflict of interest was reported by the author(s).

## ORCID

Jean N. Reinaud  <http://orcid.org/0000-0001-5449-6628>

Xavier Carton  <http://orcid.org/0000-0002-7849-6611>

## References

- Ambar, I., Serra, N., Neves, F. and Ferreira, T., Observations of the Mediterranean undercurrent and eddies in the Gulf of Cadiz during 2001. *J. Mar. Syst.* **2008**, **71**, 195–220.
- Aref, H., Motion of three vortices. *Phys. Fluids* **1979**, **22**, 393–400.
- Aref, H., Self-similar motion of three point vortices. *Phys. Fluids* **2010**, **22**, 057104.
- Aguiar, A.C.B., Peliz, Á. and Carton, X., A census of Meddies in a long-term high-resolution simulation. *Prog. Oceanogr.* **2013**, **116**, 80–94.
- Charney, J.G., Geostrophic turbulence. *J. Atmos. Sci.* **1971**, **28**, 1087–1095.
- Chelton, D.B., Schlax, M.S. and Samelson, R.M., Global observations of nonlinear mesoscale eddies. *Prog. Oceanogr.* **2011**, **91**, 167–216.
- Dong, C., McWilliams, J.C., Liu, Y. and Chen, D., Global heat and salt transports by eddy movement. *Nature Comm.* **2014**, **5**, 3294.
- Dritschel, D.G., The instability and breakdown of tall columnar vortices in a quasi-geostrophic fluid. *J. Fluid Mech.* **1996**, **328**, 129–160.
- Dritschel, D.G. and Ambaum, M.H.P., A contour-advective semi-Lagrangian numerical algorithm for simulating fine-scale conservative dynamical fields. *Quart. J. Roy. Meteorol. Soc.* **1997**, **123**, 1097–1130.
- Dritschel, D.G. and Saravanan, R., Three-dimensional quasi-geostrophic contour dynamics, with an application to stratospheric vortex dynamics. *Quart. J. Roy. Meteorol. Soc.* **1994**, **120**, 1267–1297.
- Dritschel, D.G., Reinaud, J.N. and McKiver, W.J., The quasi-geostrophic ellipsoidal vortex model. *J. Fluid Mech.* **2003**, **505**, 203–223.
- D'Addezio, J.M., Jacobs, G.A., Yaremchuk, M. and Souopgui, I., Submesoscale Eddy vertical covariances and dynamical constraints from high-resolution numerical simulations. *J. Phys. Oceanogr.* **2020**, **50**, 1087–1115.
- Gröbli, W., *Spezielle Probleme über die Bewegung Geradliniger Paralleler Wirbelfäden*, 1877 (Druck von Zürcher und Furrer: Zürich).
- Gula, J., Molemaker, M. and McWilliams, J., Topographic generation of submesoscale centrifugal instability and energy dissipation. *Nat. Commun.* **2016**, **7**, 12811.
- Hernández-Garduño, A. and Lacombe, E.A., Collisions and regularization for the 3-vortex problem. *J. Math. Fluid Mech.* **2007**, **9**, 75–86.
- Jamalooden, M.I. and Newton, P.K., Two-layer quasigeostrophic potential vorticity model. *J. Math. Phys.* **2007**, **48**, 065601.
- Kimura, Y., Similarity solution of two-dimensional point vortices. *J. Phys. Soc. Jpn.* **1987**, **56**, 2024–2030.



- Nastrom, G.D., Gage, K.S. and Jasperson, W.H., Kinetic energy spectrum of large-and mesoscale atmospheric processes. *Nature* **1984**, **310**, 36–38.
- Novikov, E.A. and Sedov, Y.B., Vortex collapse. *Sov. Phys. JETP* **1979**, **50**, 297–301.
- Özügürü, E., Reinaud, J.N. and Dritschel, D.G., Interaction between two quasi-geostrophic vortices of unequal potential vorticity. *J. Fluid Mech.* **2008**, **597**, 395–414.
- Polvani, L., Two-layer geostrophic vortex dynamics. Part 2. Alignment and two-layer V-states. *J. Fluid Mech.* **1991**, **225**, 241–270.
- Quentel, E., Carton, X. and Gutscher, M.A., Structure and temporal variability of Mediterranean water from hydrological and marine seismic data south of Portimao Canyon (Gulf of Cadiz) from 1999 to 2002. *Int. J. Geosci.* **2011**, **2**, 185–194.
- Reinaud, J.N., Self-similar collapse of three geophysical vortices. *Geophys. Astrophys. Fluid Dyn.* **2021**, **115**, 369–392.
- Reinaud, J.N. and Carton, X., The alignment of two three-dimensional quasi-geostrophic vortices. *Geophys. Astrophys. Fluid Dyn.* **2020**, **114**, 524–560.
- Reinaud, J.N., Dritschel, D.G. and Koudella, C.R., The shape of vortices in quasi-geostrophic turbulence. *J. Fluid Mech.* **2003**, **474**, 175–191.
- Reinaud, J.N., Dritschel, D.G. and Scott, R.K., Self-similar collapse of three vortices in the generalised Euler and quasi-geostrophic equations. *Phys. D* **2022**, **434**, 133226.
- Zhang, Z., Wang, W. and Qiu, B., Oceanic mass transport by mesoscale eddies. *Science* **2014**, **345**, 322–324.